COMPARISON OF NUMERICAL AND EXPERIMENTAL RESULTS OF THE AIR FLOW IN THE TEST SECTION OF AN OPEN LOW SPEED WIND TUNNEL

Soares, Cleide Barbosa, cleide_bsoares@hotmail.com
Federal Center of Technological Education of Minas Gerais-CEFET-MG, Av. Amazonas, 5.253 – Nova Suiça - Belo Horizonte, Minas Gerais, Brazil- Cep. 30480-000

Hanriot, Sérgio de Morais, hanriot@pucminas.br
Maia, Cristiana Brasil, cristiana@pucminas.br
Cabezas-Gómez, Luben, luben@pucminas.br
Pontifical Catholic University of Minas Gerais-PUC-MG, Av. Dom José Gaspar, 500 – Coração Eucarístico - Belo Horizonte, Minas Gerais, Brazil – Cep. 30535-610

Abstract. *Aerodynamic forces arise from the relationship between the relative velocity between the air and the body model. In a wind tunnel, this relative velocity is achieved moving the air over a stationary model. In the past years, several wind tunnels are being designed and built to measure aerodynamic forces and moments. It is observed that, even with the recent computational advances, wind tunnels are still an essential tool to the study of the aerodynamics. This paper presents a comparison between numerical and experimental data in the test section of a low speed wind tunnel. Numerical results were obtained for three turbulence models, namely the k-ε, RNG k-ε and shear stress transport SST models. Two boundary conditions for the outlet were evaluated. The simulation results were compared with the mean time experimental velocity profiles as a function of several values of inlet mass flow rate, as well as with the experimental turbulent kinetic energy The comparison of the numerical and experimental data showed that the SST model appears to be the one that produces the best results. Two different wind-tunnel numerical exit regions were also compared, corresponding to two different formulations of the exit boundary condition. The results showed that the extended domain condition seems to produce better numerical results.*

Keywords: *wind tunnel, hot wire anemometry, CFD, experimental analysis*

1. INTRODUCTION

A wind tunnel is a research tool used to help the study of the effects of air moving over or around a body. Geometrical shapes or models (such as cars or plane wings) are mounted inside a duct and air is blown or sucked through this duct, creating a relative movement between the air and the object. Although the first wind tunnels predated the advent of airplanes, with Wenham in 1871, the wind tunnel was developed along with the aeronautical industry, between 1900 and 1960. In this period, the wind tunnel was seen as an essentially research tool. Between 1960 and 1980, it became a reliable and robust tool for commercial design purposes. From 1980, there have been significant advances in wind tunnel testing techniques, particularly in terms of instrumentation (Baker, 2007). Even with the computational advances, wind tunnels still represent an essential tool to aerodynamic studies. Wind tunnel measurements are being used to validate Computational Fluid Dynamics (CFD) calculations, and CFD can be used as a tool to support wind tunnel design, wind tunnel testing and the interpretation of the test results (Moonen, *et.al*, 2006).

Several reports of experiments performed in wind tunnels are available in literature. Wind tunnels are used to evaluate the drag and lift forces in objects (Kämpchen, *et. al*, 2003, and Larose, D'Auteuil. 2008), to investigate mean and fluctuating wind loads on buildings and atmospheric boundary layers (Iyengar; Farell, 2001, Farell; Iyengar, 1999 and Zhang , Gu, 2008) and to investigate turbulent boundary layers (Finnveden, *et. al*, 2005), among other studies.

With the improvement of computational capabilities, CFD techniques have been used to predict the behavior of the airflow over and around solid bodies and to predict the acting forces and moments over them. Experiments in wind tunnels are performed to validate the numerical models (Cluni, *et. al*, 2008 and Gromke *et. al*, 2008).

This paper presents numerical and experimental investigations of the airflow inside an open wind tunnel. Experimental tests were performed in the test section of a low-speed wind tunnel. Velocity and pressure were measured in an array of points in the test section. The instantaneous velocity and turbulent intensity were measured in the central point of the exit region of test section with a hot-wire anemometer. Numerical results were obtained using three turbulence models: the standard *k-ε*, the *RNG k-ε* and the *SST* model. Two boundary conditions were evaluated for the outlet region.

2. METHODOLOGY

2.1. Numerical Methodology

A Computational Fluid Dynamics (CFD) technique comprehends the numerical solution of the governing flow equations. In the analysis, the solution domain is divided into a large number of infinitesimal control volumes and the governing equations are solved for each of them. In this work, the main governing equations of fluid flow considered were mass and momentum conservation.

For turbulent flows, it is necessary to take into account the effects of turbulence. In this paper it is done through application of turbulence models. Three turbulence models were evaluated: *k-ε* model (Cluni *et. al*, 2008), the *RNG k-ε* model (Yakhot *et. al*, 2008) and the *SST* model. The *SST* model was proposed by (Menter, 1994) from the *k-ω* turbulence model, initially formulated by (Wilcox, D. C., 1993). The models are presented in the above-mentioned order, considering only the main equations used in the numerical simulations. Models constants are also introduced. It is important to note that are presented the model definitions and formulation used in (ANSYS, 2008), since the numerical simulations were performed with this commercial code. The main interest is to study how different models can lead to different computational results only considering the defaults definition of each model, including the default boundary conditions.

The mass conservation and momentum conservation equations are used in the same form for all the models evaluated.

Mass conservation:

$$\frac{\partial \rho}{\partial t} + \vec{\nabla} \cdot (\rho U) = 0 \tag{1}$$

where ρ represents the specific mass of the fluid and U is the vector of velocity.

Momentum conservation:

$$\frac{\partial (\rho U)}{\partial t} + \vec{\nabla} \cdot (\rho U \otimes U) - \vec{\nabla} \cdot \left(\mu_{eff} \vec{\nabla} U\right) = -\vec{\nabla} p' + \vec{\nabla}\left(\mu_{eff} (\vec{\nabla} U)\right)^T + B \tag{2}$$

where *B* is the sum of body forces, μ_{eff} is the effective viscosity accounting for turbulence, and *p'* is the modified pressure. μ_{eff} and *p'* are given respectively by:

$$\mu_{eff} = \mu + \mu_t \tag{3}$$

$$p' = p + \frac{2}{3}\rho k \tag{4}$$

The Reynolds number used in the Results section is:

$$Re = \frac{\rho . Q}{\mu . b} \tag{5}$$

where Q is the volume flow rate (m^3/s), μ is the absolute viscosity (kg/m.s) and *b* is the width of the test section (m).

2.2. Standard *k-ε* model

The *k-ε* model uses the eddy viscosity concept, assuming that the turbulence viscosity μ_t is computed by:

$$\mu_t = C_\mu \rho \frac{k^2}{\varepsilon} \tag{6}$$

Where C_μ is a model constant.

The standard *k-ε* model (Wilcox, 1993) introduces two new variables into the equation system: the turbulent kinetic energy, *k*, m^2/s^2; and the turbulence eddy dissipation,*ε*, m^2/s^3. The new variables are obtained through the solution of transport equations, given by:

$$\frac{\partial(\rho k)}{\partial t} + \vec{\nabla}\cdot(\rho U k) = \vec{\nabla}\cdot\left[\left(\mu + \frac{\mu_t}{\sigma_k}\right)\vec{\nabla}k\right] + P_k - \rho\varepsilon \tag{7}$$

$$\frac{\partial(\rho \varepsilon)}{\partial t} + \vec{\nabla}\cdot(\rho U \varepsilon) = \vec{\nabla}\cdot\left[\left(\mu + \frac{\mu_t}{\sigma_\varepsilon}\right)\vec{\nabla}\varepsilon\right] + \frac{\varepsilon}{k}\left(C_{\varepsilon 1}P_k - C_{\varepsilon 2}\rho\varepsilon\right) \tag{8}$$

In the equations, $C_{\varepsilon 1}$, $C_{\varepsilon 2}$, σ_k and σ_e are the model constants and P_k is the turbulence production tensor due to viscous forces. The buoyancy forces are not considered in the present work.

The *RNG k-ε* model is based on renormalization group analysis of the Navier-Stokes equations. The transport equations for turbulence generation and dissipation are the same as those for the standard *k-ε* model, but the model constants differ. The equations for the momentum and continuity are also the same.

The other two-equation turbulence model refers to the Shear Stress Transport model taken from (Launder, 1974). This model was proposed by (Menter, 1994), and grew from the denominated baseline *k-ω* model in (Launder, 1974). The baseline *k-ω* model makes use of the *k-ε* model in regions far away from the walls and the *k-ω* Wilcox model (Wilcox, 1993) near the surface. The *SST* model is an improvement of the baseline *k-ω* model, taking into account the transport of the turbulent shear stress by a limitation of the eddy viscosity ν_t by the following equation:

$$\nu_t = \frac{a_1 k}{\max(a_1 w, SF_2)} \tag{9}$$

Where: $\nu_t = \mu_t/\rho$ and *S* represents an invariant measure of the strain rate. F_2 is a blending function, which restricts the limiter to the wall layer computed by:

$$F_2 = \tanh(\arg_2^2) \tag{10}$$

with:

$$\arg_2 = \max\left(\frac{2\sqrt{k}}{\beta' \omega y}, \frac{500\nu}{y^2\omega}\right) \tag{11}$$

where β' is a coefficient equals to 0.09.

3. EXPERIMENTAL SETUP

The experiments were conducted in the 200 mm wide x 200 mm high x 790 mm long test section of the open wind tunnel shown in Fig. 1. Before the test section removable grids can be installed to homogenize the flow turbulence. The rotational speed of the fan is controlled to modify the mass airflow inside the wind tunnel. The tests were carried out for several values of rotational speeds, ranging from 1800 rpm up to 3200 rpm.

In order to measure the mean time axial velocity a Pitot-static probe was used in several points of the exit test section region. Considering that (ISO 3966:1977) establishes a minimum of 25 measurement points, 36 measurement points were used to characterize the velocity profile in the exit of the test section. These points are shown in Fig. 2, where (0, 0) corresponds to the centre of the section and the values are in mm.

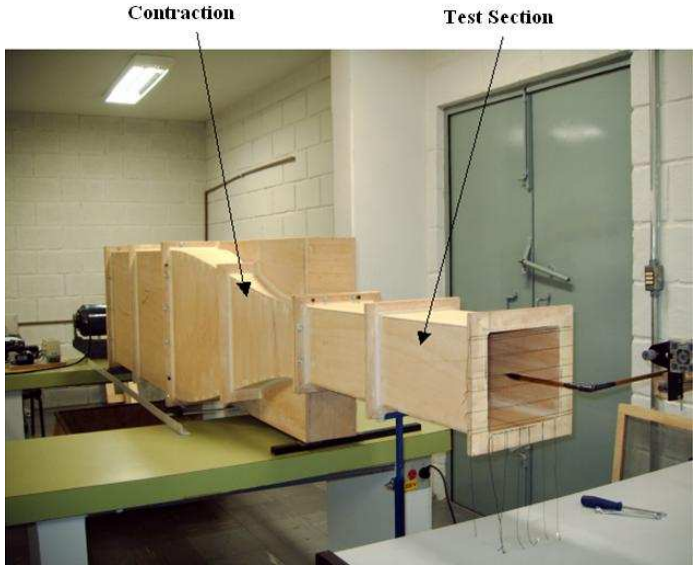

Figure 1. Wind tunnel (Soares, 2008)

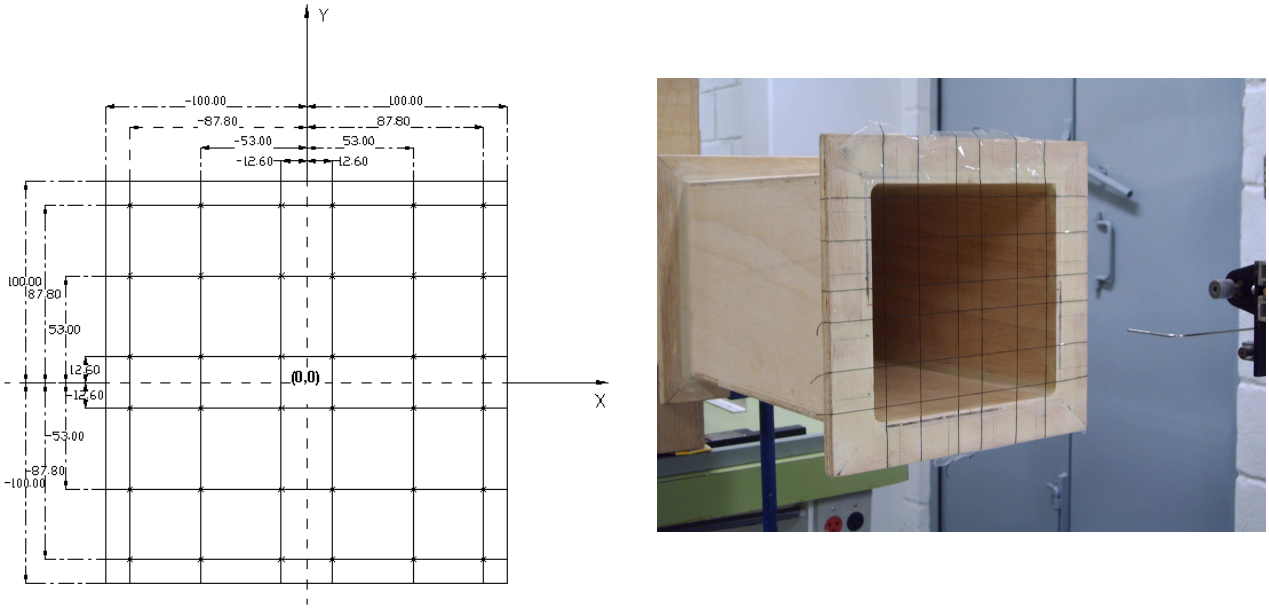

Figure 2. Velocity measurement points at the exit of the test section (Soares, 2008)

A hot wire anemometer was placed in the centre of the test section (0,0 coordinates) to evaluate the instantaneous velocity and the intensity of turbulence of the airflow at this point. In the experiments, the room temperature was 293 K and the atmospheric pressure was 90.6 kPa.

4. RESULTS AND DISCUSSIONS

Numerical results were obtained for the same conditions of the experimental data, 90.6 kPa and 293 K. Three rotational speeds of the fan were simulated: 1800 rpm, 2500 rpm and 3200 rpm, corresponding to volume flow rates of 0.19 m^3/s, 0.27 m^3/s and 0.34 m^3/s, respectively. The Reynolds numbers for the rotational speeds were $5.7x10^4$, $8.1x10^4$ and $1.0x10^5$, respectively.

The airflow was simulated in the test section of the wind tunnel. A mass flow rate, obtained from experimental results, was used as inlet boundary condition. For the turbulent variables a medium intensity (5%) of turbulence was adopted (ANSYS, 2008). A no-slip boundary condition was considered for the wind tunnel test section walls. The flow was assumed as isothermal with a temperature of 293 K. The turbulence models constants were also assumed as the default values considered in the CFX code.

In the exit region of the test section, two different geometrical configurations and boundary conditions were evaluated. In the first case, the computational domain was the same of the wind tunnel prototype test section. In the exit section, a CFX outlet boundary condition was specified with a zero value for the relative pressure. For the second case,

an additional region was used after the wind tunnel exit (see Figures 7 and 9). In this additional region was considered a zero value of the relative pressure in all outlet surfaces and a CFX opening condition was set out. This condition allows an inward and outward mass flow across the outlet surfaces. These two different boundary conditions were set out in order to study the influence of the outlet boundary condition on the numerical results. As it is known from literature, the mathematical and numerical modeling of this kind of boundary condition in wind tunnels is a difficult task. In the present work are presented some results in order to show briefly how the numerical results can differ in either case.

For the first computational domain (i.e. the first outlet boundary condition), it was employed a computational mesh with a total number of elements and nodes of 463071and 120371, respectively (Fig.3a). For the second domain, the total number of elements and nodes employed were 1386313 and 339286, respectively (Fig.3b). The results were obtained using an Intel Core 2 Duo E4600 Processor with 2.4 GHz and 1.0 Gb of RAM. The time required for the numerical simulations was 22 minutes for the first exit boundary condition and 84 minutes for the second exit boundary condition.

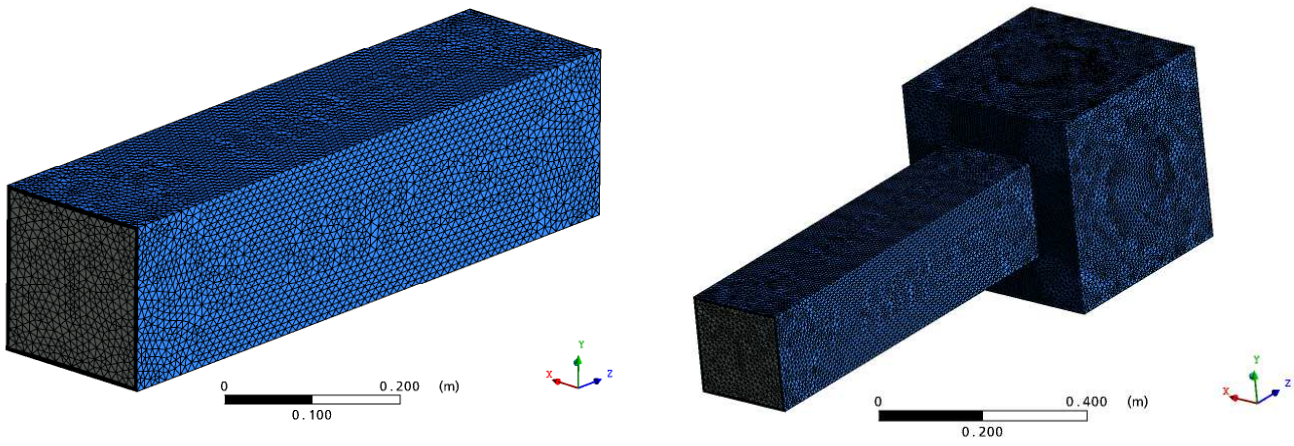

(a) (b)

Figure 3. Computational mesh for the first (a) and second (b) exit boundary condition.

Figures 4 and 5 show the numerical results and experimental data of the cross-sectional mean time axial velocity profiles at position (x = 0.1126 m, $0 \leq y \leq 0.2$ m) in the exit plane of the wind-tunnel test section. The profile for the first exit region is shown in Fig. 4 and for the computational domain, with the additional exit region, is shown in Fig. 5. In terms of the mean time axial velocity, it is not observed significant differences in the numerical results obtained for each turbulence model and each fan rotational speed, neither for the exit tunnel computational regions or exit boundary conditions evaluated. In the present case this behavior is expected because the flow does not present a strong adverse pressure gradient at the exit region, which commonly lead to unsatisfactory results when the k-ε and *RNG* k-ε models are used (Menter, 1994).

Comparing with the experimental data, the major differences are observed in the regions near the tunnel walls, especially in the left side. This behavior can be explained to small distortions of the wood wind tunnel walls; which produce an asymmetry of the experimental velocity profiles.

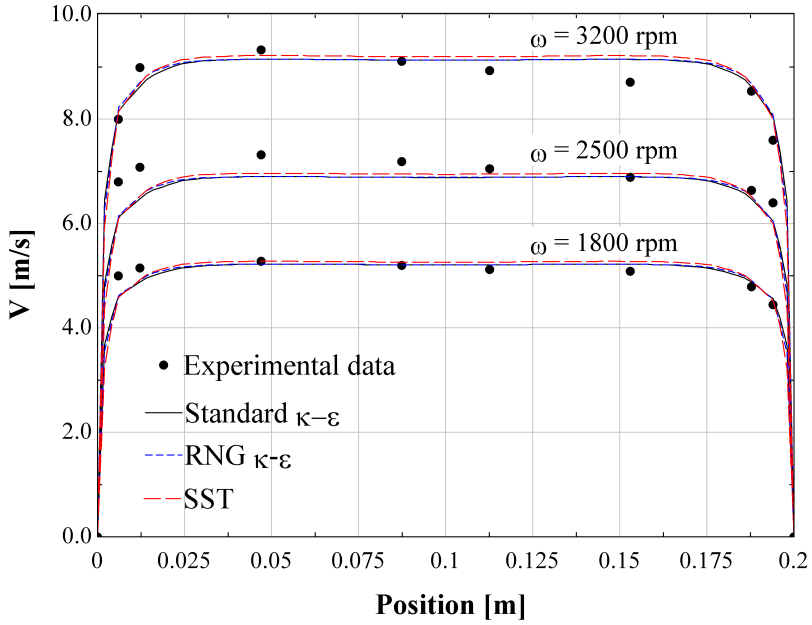

Figure 4. Velocity profile versus position at exit wind tunnel section for the first exit boundary condition.

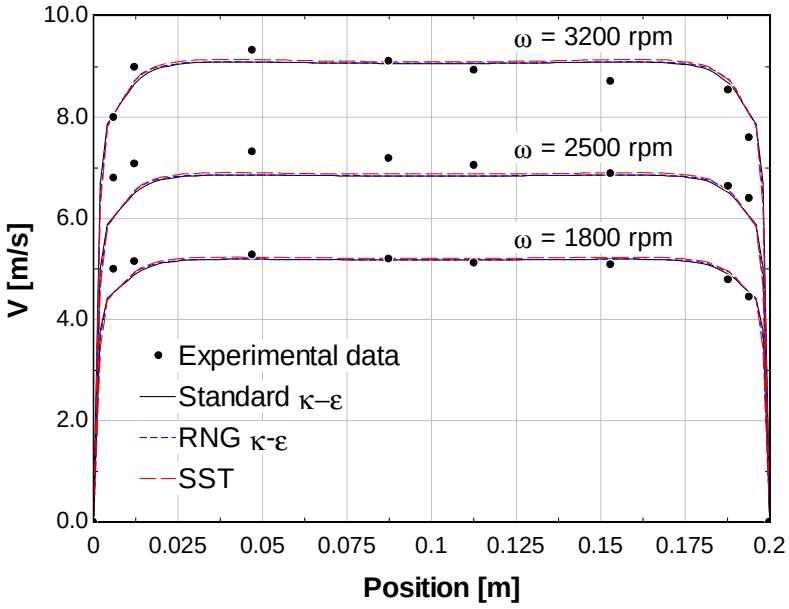

Figure 5. Velocity profile versus position at exit wind tunnel section for the second exit boundary condition.

The turbulent kinetic energy profiles for the three turbulence models are shown in Fig. 6 (first exit boundary condition) and Fig. 7 (second exit boundary condition), for a rotational speed of 2500 rpm. The experimental data was obtained in the centre of the tunnel using the hot wire anemometer sensor. The turbulent kinetic energy is associated with the rms velocity fluctuations. Using a hot wire anemometer, Laufer (1954) showed that the rms fluctuations in a turbulent developed pipe flow are small in the regions near walls and have a sharp maximums near the edges of the laminar sub layers, existing a strong movement of kinetic energy away from this point (laminar sub layer). This behavior was obtained only with the *SST* turbulence model, as shown in Fig.6 and 7. The *k-ε* and *RNG k-ε* models were not able to predict this feature. Considering the experimental value of the turbulent kinetic energy in the tunnel centre it is also noted that the best prediction was obtained with the *SST* model. It can be noticed that, with the second exit boundary condition, the values of the turbulent kinetic energy near the wall were lower for the SST model and higher for the *k-ε* and *RNG k-ε* models. Similar behaviours were obtained for the other rotational speeds.

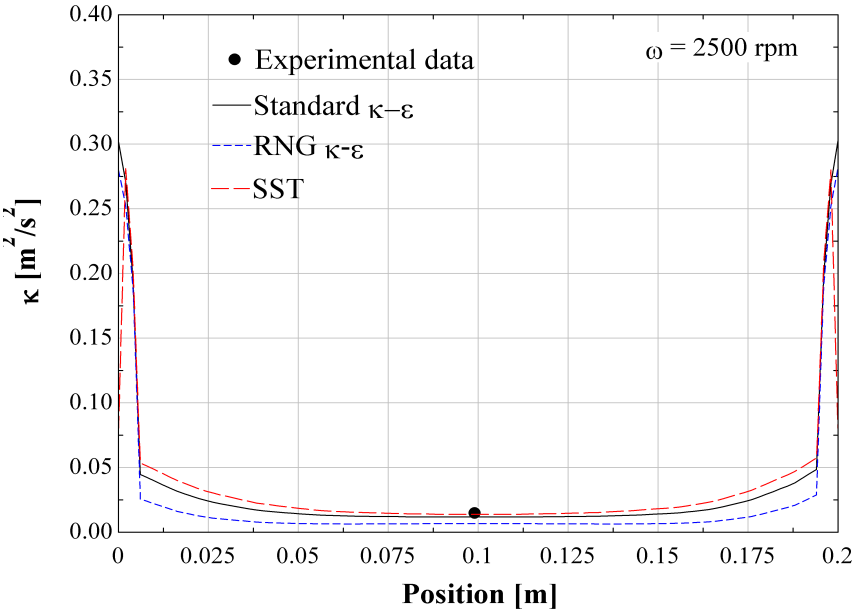

Figure 6. Turbulent kinetic energy versus position at exit section for the first exit boundary condition.

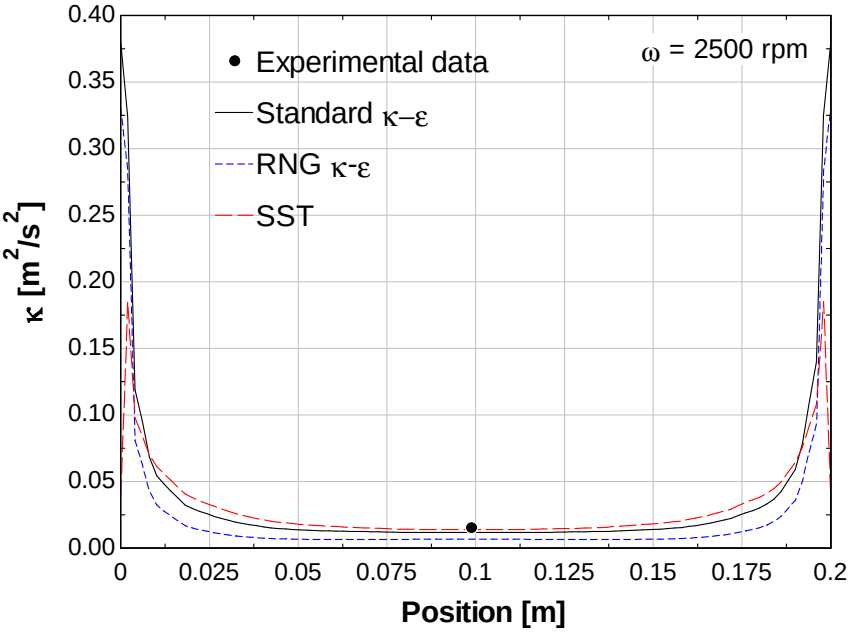

Figure 7. Turbulent kinetic energy versus position at exit section for the second exit boundary condition.

Figures 8 and 9 show the numerical velocity field in the test section of a wind tunnel for the first and second exit boundary conditions, respectively, for a rotational speed of 3200 rpm. For the second exit boundary condition (Fig. 9), it can be seen a free jet and a recirculation region in the outlet section after the test section, properly of this type of flow. It can be noticed the resemblance between the velocity fields obtained for both boundary conditions. However in the first case (Fig. 8) it is not possible to simulate the free jet exit region, being numerically imposed a developed flow at the exit region. This approach can cause certain deviations of the computed turbulent quantities and flow details, because the flow in the exit region could not be well developed due to the shearing phenomena of the exit free jet with the surrounding stagnant air. In order to better understand this phenomenon, more refined simulations, as well as experimental measurements, are needed. These tasks are under development. The maximum velocity in both cases is equal to 9.23 m/s and 9.18 m/s, respectively, in accordance with experimental data.

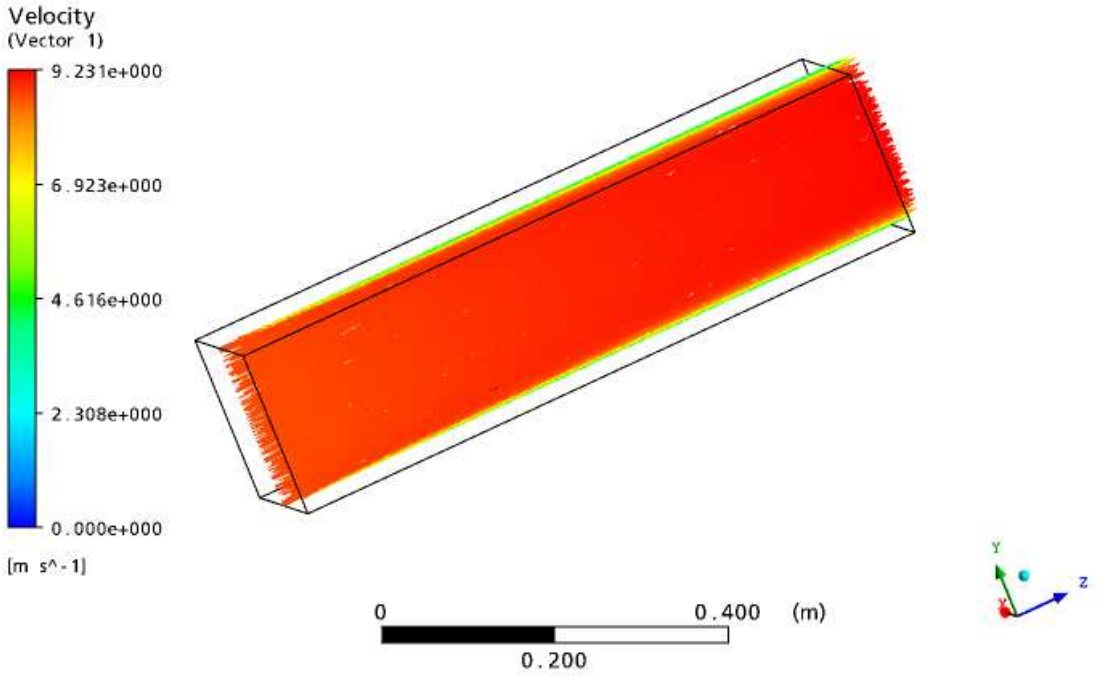

Figure 8. Numerical results of velocity field in the middle tunnel section for the first exit boundary condition

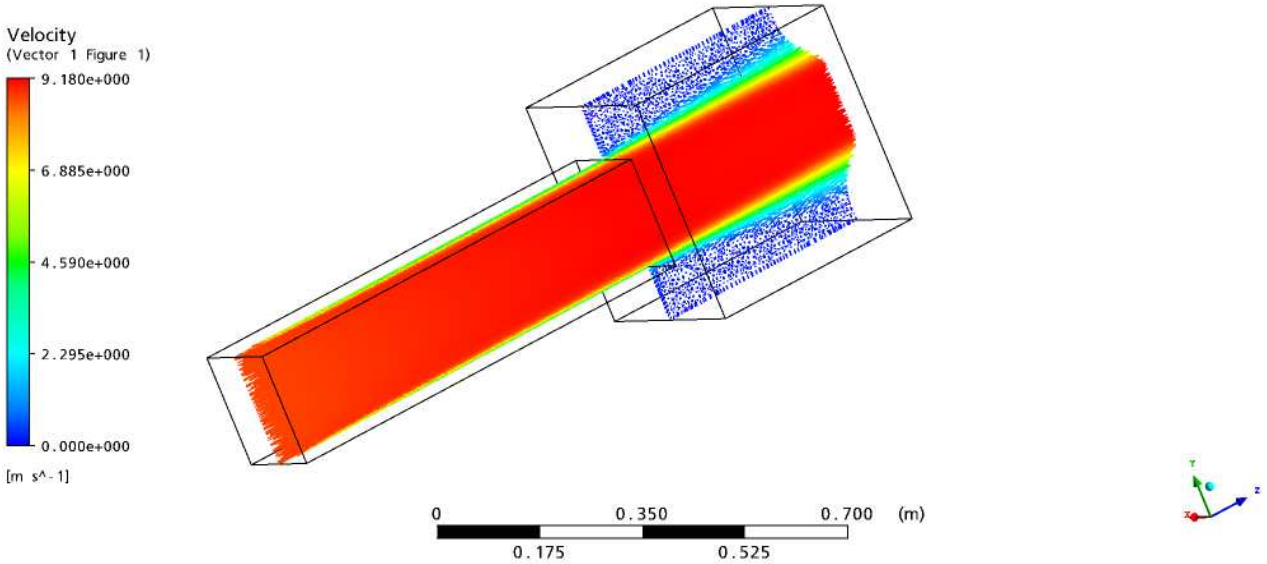

Figure 9. Numerical results of velocity field in the middle tunnel section for the second exit boundary condition

Figures 10 and 11 show the numerical pressure field in the test section of wind tunnel for the boundary conditions adopted, for a rotational speed of 3200 rpm. It can be seen that the highest relative pressure is at the inlet of the test section, decreasing towards the exit region, as expected. It should be observed that the present turbulent flow is characterized by very small pressure gradient and relative pressure values, which were not possible to measure experimentally with the available measurement devices. However, the displayed pressure gradient seems to be physically correct, and will be validated in future works.

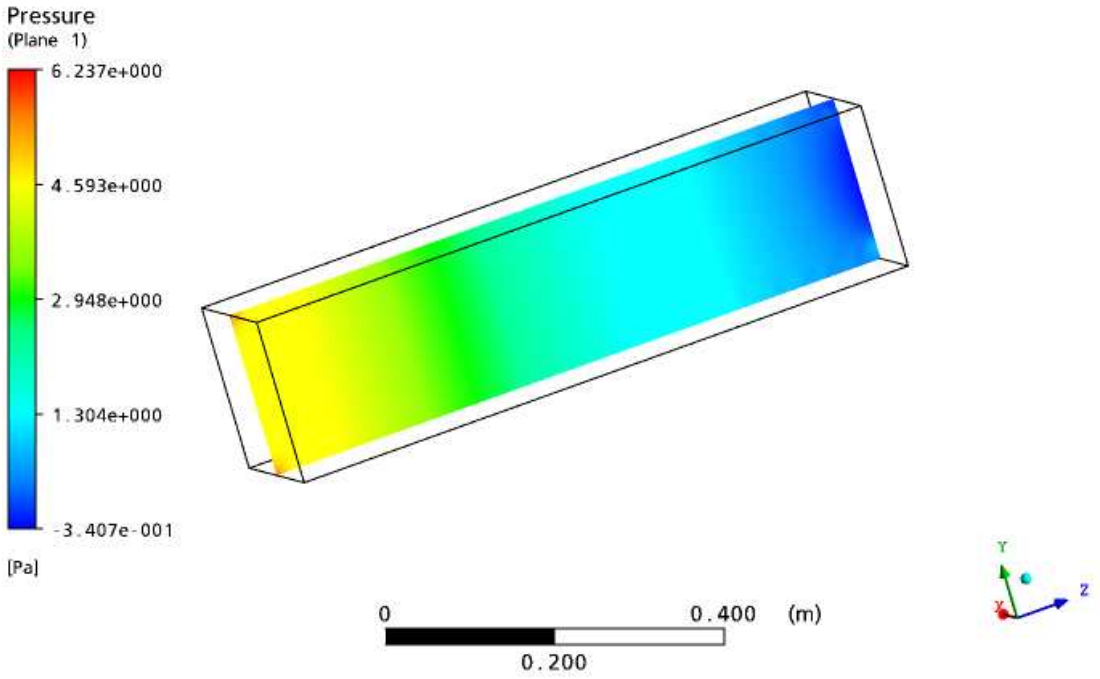

Figure 10. Numerical results of pressure field in the middle tunnel section for the first exit boundary condition

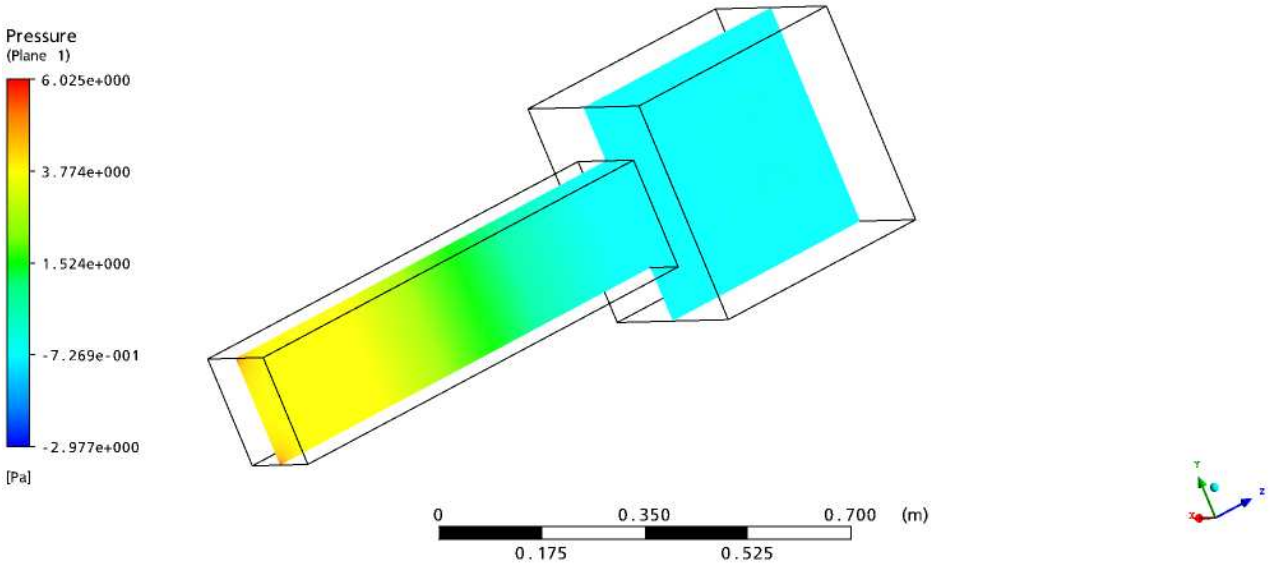

Figure 11. Numerical results of pressure field in the middle tunnel section for the second exit boundary condition

5. CONCLUSIONS

This paper presents a comparison between numerical and experimental data in the test section of a low speed wind tunnel. Detailed Pitot tube and hot wire anemometry measurements were made to examine the flow behavior in the exit region of a wind tunnel build from wood. Numerical results were obtained for three turbulence models, namely the *k-ε*, *RNG k-ε and* shear stress transport *SST* models. The simulation results were compared with the mean time experimental velocity profiles as a function of three values of inlet mass flow rate, as well as with the experimental turbulent kinetic energy in the centre of the exit region of wind tunnel. The comparison of the numerical and experimental data showed that the *SST* model appears to be the one that produces the best results. More advances studies must be carried on to confirm the present observations.

In the paper are also compared two different wind-tunnel numerical exit regions, corresponding to two different formulations of the exit boundary condition. It seems that the extended domain condition produces better numerical results, because of the possibility of simulating the free jet formed at the exit region of the wind tunnel. Nevertheless, more results are needed to fully support this conclusion.

6. ACKNOWLEDGMENTS

Authors are grateful to Foundation for the Support of Research of the State of Minas Gerais-Brazil (FAPEMIG), to National Council for Scientific and Technological Development (CNPQ), Federal Center of Technological Education of Minas Gerais (CEFET-MG) and Pontifical Catholic University of Minas Gerais (PUC Minas), who supports this work.

7. REFERENCES

ANSYS, 2008, ANSYS-CFX® Solver Theory manual, Release 11.0.

Iyengar, A.K.S.; Farell, C., 2001, "Experimental issues in atmospheric boundary layer simulations: roughness length and integral length scale determination". Journal of Wind Engineering and Industrial Aerodynamics pp.1059–1080

Farell, C.S.; Iyengar, A.K.S., 1999, "Experiments on the wind tunnel simulation of atmospheric boundary layers". Journal of Wind Engineering and Industrial Aerodynamics pp. 11-35.

Baker, C.J. Wind engineering, 2007, "Past, present and future". Journal of Wind Engineering and Industrial Aerodynamics pp. 843–870

Gromke, C.; Buccolieri, R.; Sabatino, S.; Ruck, B. 2008, "Dispersion study in a street canyon with tree planting by means of wind tunnel and numerical investigations" – Evaluation of CFD data with experimental data. Atmospheric Environment Volume 42, Issue 37, pp. 8640-8650.

Cluni, F.; Gusella, V.; Bartoli, G. 2008, "Wind tunnel scale model testing of suspended cables and numerical comparison". Journal of Wind Engineering and Industrial Aerodynamics pp.1134–1140

Larose, G.L.; D'Auteuil, A. 2008, "Experiments on 2D rectangular prisms at high Reynolds numbers in a pressurised wind tunnel". Journal of Wind Engineering and Industrial Aerodynamics pp. 923–933

INTERNATIONAL ORGANIZATION for STANDARDIZATION. ISO 3966:1977 – Measurements of fluid flow in closed conduits velocity area method using Pitot static tubes- First Edition.

Launder, B. E. and Spalding, D. B., 1974. The Numerical Computation of Turbulent Flows. Comput. Methods Appl. Mech. Eng., 3: pp.269-289.

Laufer, J., 1954 The structure of turbulence in fully developed pipe flow, NACA report pp.1174.

Menter, R. F.,1994, "Two-equation Eddy-viscosity Turbulence Models for Engineering Applications". AIAA Journal. 32(8): pp.269-289 .

Kämpchen, M.; Dafnis, A.; Reimerdes, H.-G.; Britten, G.; Ballmann, J.; 2003,"Dynamic aero-structural response of an elastic wing model. Journal of Fluids and Structures pp.63–77

Moonen, P.; Blocken, B.; Roels, S.; Carmeliet, J.; 2006, "Numerical modeling of the flow conditions in a closed-circuit low-speed wind tunnel". Journal of Wind Engineering and Industrial Aerodynamics pp. 699–723

Finnveden, S.; Birgersson1, F.; Ross, U.; Kremer, T.; 2005, A model of wall pressure correlation for prediction of turbulence-induced vibration. Journal of Fluids and Structures, pp.1127–1143

Soares, C. B., 2008, Experimental Study of the Velocity Profiles in Test Section of an Open Low Speed Wind Tunnel 2008. 138f. Master degree dissertation, Pontifical Catholic University of Minas Gerais, Belo Horizonte, Brazil.

Wilcox, D. C., 1996, Turbulence Modeling for CFD. DCW Industries, La Cañada, CA, 1993. ANSYS-CFX® Solver Theory manual, Release 10.0.

Liu, X.; Levitan, M.; Nikitopoulos, D. "Wind tunnel tests for mean drag and lift coefficients on multiple circular cylinders arranged in-line". Journal of Wind Engineering

Yakhot, V., Orszag, S. A., Thangam, S., Gatski, T. B. and Speziale, C. G., 1992,Development of Turbulence Models for Shear Flows by a Double Expansion Technique. Physics of Fluids A. 4(7): pp.1510-1520.

Zhang, A., Gu, M., 1996, "Wind tunnel tests and numerical simulations of wind pressures on buildings in staggered arrangement". Journal of Wind Engineering and Industrial Aerodynamics 96 pp. 2067–2079.

8. RESPONSIBILITY NOTICE

The authors are the only responsible for the printed material included in this paper.